RSC Advances

PAPER

View Article Online
View Journal | View Issue

Cite this: *RSC Adv.*, 2017, **7**, 49505

A theoretical investigation of the two-photon absorption and fluorescent properties of coumarin-based derivatives for Pd^{2+} detection†

Chun Zhang,[a] Jing-Fu Guo,[b] Ai-Min Ren *[a] and Dan Wang[c]

Palladium is emitted due to automobile catalytic converters, and with rapid growth in the number of cars, palladium is thus a current threat to human health and the environment. Two-photon (TP) fluorescent probes are favorable and powerful molecular tools for palladium ion (Pd^{2+}) detection due to localized excitation and reduced phototoxicity and photodamage. In the present study, a series of "turn-on" TP fluorescent dyes based on coumarin derivatives were designed for Pd^{2+} recognition. Our study revealed the origin of the peculiarly different fluorescence behaviors of the synthesized Pd^{2+} probe R1 and the product P′1 quantitatively and qualitatively from a theoretical perspective. Moreover, quantum-chemical calculations on electronic structures, one/two-photon absorption and fluorescence optical properties have first been carried out for these TP fluorescent chromophores using an *ab initio* approach. The calculated results demonstrate that chemical modifications of the coumarin core by the introduction of an electron-withdrawing group (–Cl or –CN) to its 4-position effectively increase the TP absorption cross-section per molecular weight more easily than extending the π-conjugated structure at the 3-position. In the present work, the product P′4, with a much smaller internal conversion rate ($K_{IC} = 1.28 \times 10^6$ s^{-1}) than that of the Pd^{2+} probe R4 ($K_{IC} = 9.09 \times 10^{11}$ s^{-1}), possesses the largest TP absorption cross-section per molecular weight (3.91) and the longest fluorescence wavelength (590.3 nm) among all the studied molecules, which means it has better potential for Pd^{2+} detection. Consequently, we hope that this detailed study can provide guidance for the design and synthesis of new Pd^{2+} fluorescent probes.

Received 10th August 2017
Accepted 5th October 2017

DOI: 10.1039/c7ra08832a

rsc.li/rsc-advances

1. Introduction

Significant amounts of palladium are emitted due to automobile catalytic converters and the rapid growth in the number of cars. As one of the platinum-group elements, palladium is hazardous to human health once it is taken up by the human body *via* contaminated water, medicine and food.[1] In the natural environment, palladium has three states: Pd^0 (metallic), Pd^{2+}, and Pd^{4+}. Its metallic form has little *in vitro* cytotoxicity, but Pd ions are capable of causing a series of cytotoxic effects, such as serious eye or primary skin irritation.[2] Epidemiological studies have indicated that Pd ions, particularly from $PdCl_2$, are the most common reactive sensitizers among metals (ranking second behind nickel). Moreover, proteins, DNA and other biomacromolecules, such as vitamin B6, have been reported to be able to strongly bind palladium ions, which may cause a variety of cellular dysfunction processes.[3,4] It is noteworthy that governmental regulations on the levels of palladium (no more than 5–10 ppm) are fairly strict and the proposed dietary intake is less than 1.5–15 μg per person per day.[5] Considering the serious threat of Pd^{2+} to the environment and human health, investigations of methodologies for the highly sensitive and selective detection of Pd^{2+} have attracted more and more attention from researchers.

Up to now, conventional methods have been developed for the efficient detection of palladium ions, including atomic absorption spectrometry, plasma emission spectroscopy, solid phase microextraction–high performance liquid chromatography, and X-ray fluorescence.[2] These methods, however, usually require expensive instruments, complicated operation and highly skilled individuals. In contrast, colorimetric and fluorimetric methods can avoid these deficiencies while maintaining comparable efficiency and accuracy; therefore, they have been widely exploited by researchers for the detection of a variety of targets.[6] Yet most of the reported Pd^{2+} fluorescent probes are excited by one-photon (OP) excitation with a short wavelength, which leads to obvious shortcomings, such as poor

[a]*Institute of Theoretical Chemistry, Laboratory of Theoretical and Computational Chemistry, Jilin University, Changchun, 130023, China. E-mail: aimin_ren@yahoo.com*

[b]*School of Physics, Northeast Normal University, Changchun, 130021, China*

[c]*MOE Key Laboratory of Macromolecular Synthesis and Functionalization, Department of Polymer Science and Engineering, Zhejiang University, Hangzhou 310027, China*

† Electronic supplementary information (ESI) available. See DOI: 10.1039/c7ra08832a

shallow tissue penetration depth, photobleaching and a high autofluorescence background.[7–9] To overcome these problems, it is urgent to develop novel two-photon (TP) fluorescent probes that are excited by two photons with longer wavelength laser light to provide an improved three-dimensional imaging resolution with increased imaging depth (>500 μm) and little photodamage to living tissue.

Coumarins have fascinated humans from the very beginning.[10] Coumarin is a conformation-restricted form of a *cis*-cinnamic acid ester, thus it has high photostability, but coumarin itself shows a poor fluorescence quantum yield and TP response. However, in very recent years so-called expanded coumarins have been synthesized, effectively expanding the portfolio of existing architectures, and great efforts have been made so far to modulate their absorption from 300 nm to 550 nm, making coumarin derivatives emit strong fluorescence in the near-infrared (NIR) region and possess tunable TPA cross-sections.[11] These π-expanded coumarin molecules have already been utilized in TP excited fluorescence microscopy.[11] In addition, a unique family of rigid analogues P′1 (GCTPOC) possessing one coumarin moiety combined with a heterocyclic moiety was reported by Lin and coworkers.[12] Importantly, P′1 as a product molecule has successfully been applied to detect a variety of biological species by TP fluorescence.[12–16] The corresponding fluorescent probes with the product molecule P′1 show good photostability, high selectivity and sensitivity, low cytotoxicity and high biocompatibility. Additionally, another coumarin derivative, P′5 (3-benzothiazol-7-hydroxy-2*H*-chromen-2-one (TPF)), also displays excellent optical properties, such as a high fluorescence quantum yield ($\phi = 0.36$), high photostability, and a large two-photon absorption (TPA) cross-section ($\delta^{T}_{max} = 217$ GM).[17] Consequently, the purpose of this work is to design a series of novel coumarin derivatives (based on the reported P′1 and P′5 molecules) with tunable absorption/emission spectra in the NIR region and relatively large TPA cross-section values, and more importantly, to obtain TP Pd^{2+} fluorescent probes for achieving the effective recognition of Pd^{2+}.

Additionally, so far, the detection mechanisms for Pd^{2+} are mostly based on the complexation of Pd^{2+} with ligands, or Pd^{2+}-triggered chemical catalytic reactions.[2] Yet most sensors based on the coordination mechanism have varying degrees of interference from other transition metal ions and strong fluorescence quenching due to the heavy atom effect.[18] In contrast, chromophores built on Pd^{2+}-triggered catalytic reaction mechanisms usually show better selectivity.[8,9,19] The detailed palladium-catalyzed chemical conversion is displayed in Fig. 1.[7,19–21] During the Pd^{2+} catalytic hydrolysis process, propargyl hydrolysis, alcohol ketone tautomerism and ether cleavage are important components and occur successively. In 2015, two TP Pd^{2+} fluorescent molecules (GCTPOC–Pd and GCTPOC) were reported by Lin's group,[14] based on this type of chemical reaction. The Pd^{2+} probe GCTPOC–Pd, which is termed R1 in this study for convenience, is synthesized by directly connecting a two-photon coumarin derivative fluorophore with an aryl propargyl ether recognition functional group, and is non-cytotoxic and has great biocompatibility. The Pd^{2+}-responsive group (aryl propargyl ether) is distinguished by the high sensitivity (detection limit 22 nM), good selectivity, mild reaction temperature, irreversible nature and rapid response (45 min) and has been verified to be suitable for use with living cells and tissues.[14] So far, although there are some theoretical and experimental reports for TP fluorescent probes,[22–27] there have been no theoretical research reports of TP probes based on Pd^{2+}-triggered chemical catalytic reactions and coumarin derivatives, and the relationship between the molecular structure and nonlinear absorption properties of coumarin derivatives is still unclear. This study is devoted to providing some strategies for designing a series of novel TP molecules based on coumarin cores, shown in Fig. S1† (Pd^{2+} probe molecules R1–9) and Fig. 2 (corresponding product molecules P′1–9). We further investigate their electronic structural properties and, more importantly, find out which structural modifications are beneficial for chromophores with longer excited wavelengths and stronger nonlinear responses. Additionally, our other goal is to clarify the microscopic mechanism for the "turned-on" optical signal during Pd^{2+} detection *via* quantum chemistry calculations.

2. Methodology

In this work, to select a suitable functional to optimize molecular geometries and calculate optical parameters in the ground state and excited state, we take the experimentally synthesized compounds P′1 (GCTPOC) and P′5 (TPF) as references to calculate their one-photon absorption (OPA) and emission features by means of a density functional theory (DFT) method with different functionals. The calculated OPA and emission wavelengths (λ^{o}_{max} and λ^{e}_{max}), as well as the corresponding oscillator strengths (f^{o} and f^{e}), are shown in Table S1.† Given the complexity of the practical environment and the fact that all the experimental measurements are recorded in PBS (phosphate buffered saline) solvents, complex solvation effects are considered. Taking the micro-solvation mode and research experience into consideration,[28] three explicit water molecules were added around the strongest electrophilic carbonyl oxygen of each studied molecule in the calculations; meanwhile, the implicit solvent effect was considered by a Polarizable Continuum Model (PCM) approach.[29] Comparing the calculated results of the explicit solvent model simulation with those of the implicit solvent by means of the common hybrid functional B3LYP (containing a 20% proportion of the Hartree–Fock exchange energy),[30,31] the influence of the explicit solvent environment is crucial. As we know, the M06-2X hybrid functional is excellent for dealing with weak interaction and electron transition simulations, especially for electronic excitation energies; furthermore it has successfully been applied in theoretical computation.[32,33] Thus, we performed calculations on the OPA and emission features of P′1 and P′5 using the M06-2X* functional (containing 44% HF exchange component); moreover, the calculated results are in good agreement with experimental data, shown in Table S1.† Therefore, the geometrical structures of all the studied molecules, as well as the OPA and emission spectra simulations, were fully optimized by using the M06-2X* (44% HF) hybrid functional along with the 6-31+G(d) basis set

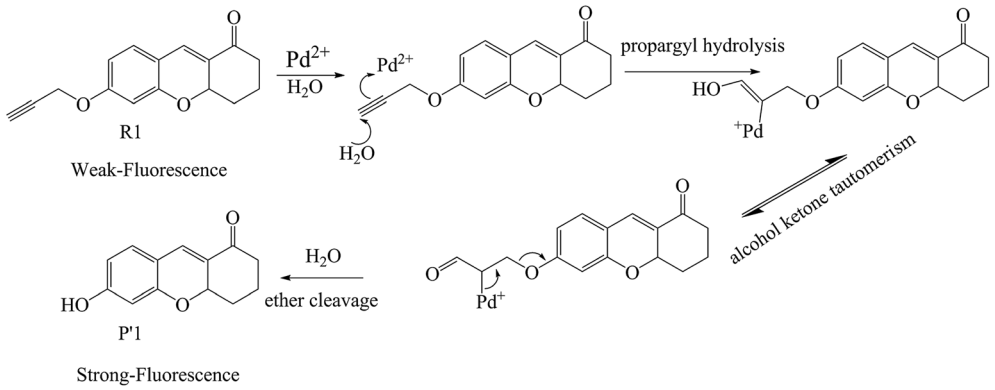

Fig. 1 The recognition mechanism of probe R1 by a Pd^{2+}-induced depropargylation reaction.

(the influence of the basis set on the spectra is displayed in Table S2†) in the implicit and explicit solvent models. Additionally, the fully optimized stationary point of a molecule can be characterized by vibrational frequency analysis to ensure that the real local minima without imaginary vibrational frequencies have been found. This vibrational frequency analysis has been successfully used in many reported investigations.[23,33–35] The vibrational frequencies of every molecule (including the explicit water molecules) at the real local minima points had positive values (listed in Table S3†) at the M06-2X* (HF = 44%)/6-

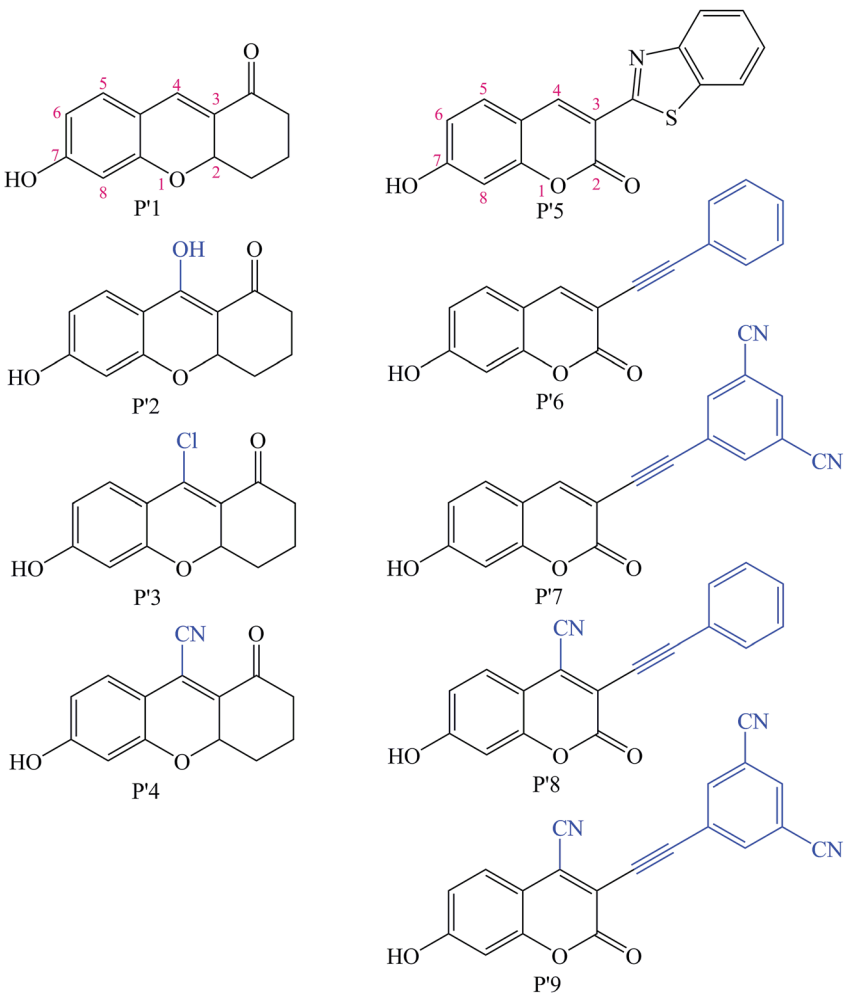

Fig. 2 Chemical structures of the modified Pd^{2+} reaction product molecules studied in this work based on the synthesized P′1 and P′5 molecules (blue groups are the modified parts).

31+G(d) level, which confirmed the stability of the different studied geometries. In order to avoid the uncertainty that the density functional may bring to the pseudo-stability, the ωB97XD functional, which is good at dealing with weak interactions, was also used to calculate the vibrational frequencies of all the studied molecules (including the explicit water molecules). The calculated results are also listed in Table S3.† The results calculated by the ωB97XD functional were also positive values, which again implied the stability of the different geometries. All of the above calculations were carried out in the Gaussian 09 program package.[36]

Furthermore, the other main task of this work is to explore the two-photon absorption (TPA) features. The TPA cross-sections (δ_{max}^{T}), which can stand for the TPA transition probability, are evaluated by the quadratic response theory using the B3LYP functional with a 6-31+G(d) basis set, as implemented in the DALTON program.[37]

Theoretically, the TP transition matrix element $S_{\alpha\beta}$ can be expressed as follows:[38]

$$S_{\alpha\beta} = \sum_i \left(\frac{\langle 0|\mu_\alpha|i\rangle\langle i|\mu_\beta|f\rangle}{\omega_i - \frac{\omega_f}{2}} + \frac{\langle 0|\mu_\beta|i\rangle\langle i|\mu_\alpha|f\rangle}{\omega_i - \frac{\omega_f}{2}} \right) \quad (1)$$

where μ_α and μ_β are the electric dipole moment operators over the molecular x, y and z axes, ω_i is the excitation energy from the ground state $|0\rangle$ to the excited state $|i\rangle$, and $\omega_f/2$ corresponds to half of the excitation energy associated with the transition from the ground to the final state $|f\rangle$. With the help of $S_{\alpha\beta}$, one can easily calculate the TP transition probability of a molecule for linearly polarized light, and the corresponding probability in the atomic unit can be written as follows:[39]

$$\delta_{TP} = 6(S_{xx}^2 + S_{yy}^2 + S_{zz}^2) + 8(S_{xy}^2 + S_{xz}^2 + S_{yz}^2) + 4(S_{xx}S_{yy} + S_{xx}S_{zz} + S_{yy}S_{zz}) \quad (2)$$

The TPA cross-section value is directly comparable with the experimental measurement and is defined as:

$$\sigma_{TP} = \frac{4\pi^2 a_0^5 \alpha\omega^2}{15 c_0 \Gamma}\delta_{TP} \quad (3)$$

where a_0 denotes the Bohr radius, α is the fine structure constant, ω stands for the energy of the excited photons, c_0 represents the speed of light and Γ represents the level broadening of the final state, which is assumed to be 0.10 eV.[40] The unit of the TPA cross-section is GM; 1 GM = 10^{-50} cm^4 s per photon. In this work, the transition dipole moment, the state dipole moment and the excitation energy are calculated using the DALTON program.

Additionally, to judge the influence of charge-transfer during the TP transitions, we calculate the charge-transfer distance (d_{CT}) and transferred charge (q_{CT}) associated with the ground and excited states using a density-based approach, which has been applied in previously reported work.[41] This density-based approach can yield more realistic charge transfer parameters, which can be used to describe the TPA properties.[42]

3. Results and discussion

3.1. Molecular design and geometry optimization of the ground state

As shown in Fig. S1† and Fig. 2, the molecules R1–9 are Pd^{2+} probes, and the molecules P′1–9 are the reaction products after Pd^{2+} treatment, respectively. In this work, the Pd^{2+} probes have a weak fluorescence signal; however, after reacting with Pd^{2+}, the product molecules have strong fluorescence spectra. Thus, we focus on systematically exploring the optical properties of the reaction products P′1–9 in this study. In order to obtain molecules with better TPA properties, the strategies of changing the substituents at different positions in the coumarin core and extending the conjugation length are adopted. Additionally, substituting groups at the other end of the fluorophore to generate a long distance from the Pd^{2+}-responsive group is very necessary, and can guarantee the high sensitivity of the probes.[43] Therefore, the construction is mainly considered as follows: (a) introducing different substituents (electron-donating and -withdrawing groups), such as a hydroxyl moiety (–OH), a chlorine group (–Cl) and a cyano group (–CN) at the 4-position of the P′1 framework to access P′2, P′3 and P′4, respectively, which balance the optimum electron donor/acceptor; a literature survey revealed that 4-substituted coumarin derivatives could be synthesized and that their fluorescence spectral properties are promising,[44–46] and, due to the strong electron-withdrawing nature and small structure size, –CN group substitution has been used in some biological fluorescent probes with low toxicity, especially for the successful tissue and cell imaging of organs.[24,47,48] (b) Extending the π-conjugation structure at the 3-position with a phenylacetylene moiety, such as P′6, in order to gain NIR absorption and emission wavelength compounds for better applications; (c) introducing an electron-withdrawing group at the 4-position or the benzene ring of the P′5 framework; P′7, P′8 and P′9 are designed in this way to determine that introducing an electron-withdrawing unit into the P′5 framework can increase the TPA cross-sections. Meanwhile, due to the electronegativity of the oxygen atom in the carbonyl group under the polarization effect, weak hydrogen bond interactions are formed between the carbonyl group and water molecules, as shown in Fig. S2 and S3† in the explicit solvent model simulation, thus the solubility of all the studied molecules should be favorable.

The optimized molecular equilibrium geometries in the ground state are shown in Fig. S2 (Pd^{2+} probe molecules) and S3 (product molecules).† Frequency calculations suggest that the equilibrium geometries are stable. P′1 and P′5 are the synthesized product molecules.[14,17] In our previous work, the explicit solvent model was considered,[33] which revealed a significant influence on the OPA and TPA features. Thus, here explicit water molecules are also added to the studied molecules. For all the studied product compounds, the fluorophore frameworks are nearly planar, which is beneficial for reducing non-radiative transitions and increasing the fluorescence quantum yield. Furthermore, the greater rigidity of the structures of the studied compounds contributes significantly to the improvement of the

nonlinear optical properties, which will be discussed in detail in the TPA properties section. Finally, considering the smaller diameter of the designed probes (maximum diameter 18.9 nm), we believe that the designed molecules have the potential to pass through the cell membrane to recognize Pd^{2+} like the synthesized probe R1.

3.2. Electronic structural properties

The energies of the highest four occupied frontier molecular orbitals and the lowest four virtual frontier molecular orbitals, as well as the energy gap (ΔE_{H-L}) between the highest occupied molecular orbital (HOMO) and the lowest unoccupied molecular orbital (LUMO), are schematically described in Fig. 3. The calculated results suggest that the ΔE_{H-L} value of P′2 is larger than that of P′1, and is the largest among all the studied products. This shows that introducing an electron-donating group at the 4-position increases the transition energy, blue-shifts the optical wavelength and is inappropriate for designing NIR fluorescent probes here. Besides, introducing an electron-withdrawing unit at the 4-position using chlorine or cyano groups can reduce the ΔE_{H-L} values, such as P′4 (2.72 eV) < P′3 (3.17 eV) < P′1 (3.27 eV), demonstrating that the electron-withdrawing group substitution at the 4-position is conducive to the decrease of ΔE_{H-L}. Substituting an electron-withdrawing group on the P′5 core also has an obvious influence on the decrease of ΔE_{H-L}. The energy gaps decrease in the order of P′5 (3.37 eV) > P′7 (2.99 eV) > P′8 (2.78 eV) > P′9 (2.20 eV), and similar changing trends also occur in their LUMO energy. Additionally, by modifying the molecular structures at the 3-position with an extended phenylacetylene π-conjugation moiety, the HOMO and LUMO energies are significantly decreased, for example P′6 ($E_{HOMO/LUMO} = -6.11/-3.02$ eV) < P′5 (−5.58/−2.21 eV), and the ΔE_{H-L} value is also reduced. Following cyano and phenylacetylene substitution, P′9 exhibits the smallest ΔE_{H-L} value and largest OPA spectra (shown in the next section) compared to those of the other products P′1–8, due to the accelerated ICT process by the electron acceptor and the extended π-conjugation. The corresponding electron density plots of the HOMO and LUMO for all of the molecules are shown in Fig. S4.†

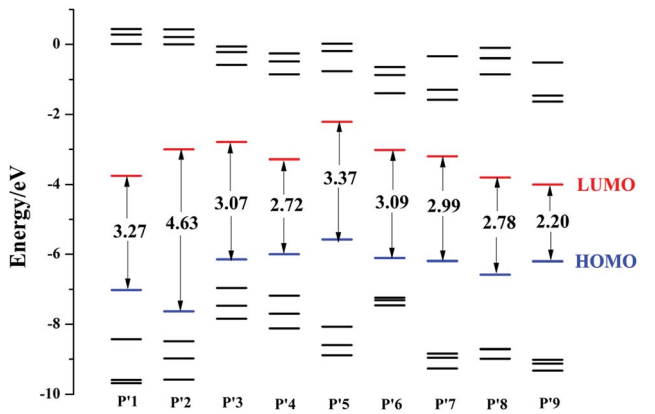

Fig. 3 Frontier molecular orbital energies of all the studied product molecules P′1–9 (The blue HOMO is the highest occupied molecular orbital, and the lower black lines are HOMO−1, HOMO−2 and HOMO−3, successively; the red LUMO is the lowest unoccupied molecular orbital, and the higher black lines are LUMO+1, LUMO+2, LUMO+3, successively. The ordinates are the corresponding energies of all the frontier molecular orbitals. The arrows represent the energy gap ΔE_{H-L} between the HOMO and LUMO).

3.3. One-photon absorption (OPA) properties

The one-photon absorption (OPA) properties of all the studied molecules have been simulated in detail by the TDDFT//M06-2X* (HF% = 44%)/6-31+G(d) method on the basis of the equilibrium geometries. The calculated OPA wavelengths (λ^{o}_{max}) and corresponding oscillator strengths (f^{o}), as well as the corresponding transition natures and some experimental values, are listed in Table 1. The OPA wavelengths of all the studied coumarin derivatives are in the range of 360–480 nm, and these results are in good agreement with common photo-physical findings from the previous report.[11] It can be seen from Table 1 that all the designed product chromophores (P′1–9) exhibit marked spectral variation following the proper modifications, demonstrating that the chemical modifications of the coumarin core in this work can effectively tune the absorption spectra to longer wavelengths. Notably, the OPA transitions of all the studied compounds are assigned as $S_0 \rightarrow S_1$ and are composed of H → L. In addition, the main OPA band of P′2 (367.3 nm) with an electron-donor (hydroxyl) group substituted at the 4-position has a significant hypsochromic shift relative to that of P′1, while those of P′3/P′4 (428.6/451.0 nm) with electron-acceptor (chlorine/cyano) groups show a bathochromic shift. When the benzene ring at the 4-position is replaced by a stronger electron-withdrawing group unit (cyano), a larger bathochromic shift of the absorption is observed, such as P′1 (385.6 nm) < P′3 (428.6 nm) < P′4 (451.0 nm). On the other hand, the conjugated structure is also an important factor, as illustrated in Table 3. When benzothiazolium is replaced by the longer π-conjugation structure of phenylacetylene, an obvious bathochromic shift of λ^{o}_{max} (P′5: 416.6 nm < P′6: 436.5 nm) occurs. This is ascribed to the fact that the extended π-conjugation structure can reinforce the charge delocalization in the whole molecule, resulting in a decreased ΔE_{H-L} and red-shifted λ^{o}_{max}. Besides, a slight bathochromic shift also takes place according to the substitution of cyano at the phenylacetylene ring, that is, P′6 (436.5 nm) < P′7 (452.2 nm). Of particular note is that introducing a cyano group only at the 4-position core (P′8) or the 4-position and phenylacetylene ring (P′9) at the same time still turns λ^{o}_{max} to a longer wavelength. Eventually, P′9 has the longest red-shift among all the P′5 core derivatives (P′5, P′6, P′7, P′8 and P′9). It can be concluded from the above discussions that introducing an electron-acceptor cyano group or extending the π-conjugation structure is an efficient approach to obtain coumarin derivative molecules with longer excited wavelengths.

3.4. Validation of the "turn-on" fluorescence of the synthesized probe and product

As reported by Lin's group, the Pd^{2+} probe R1 shows weak fluorescence, while the recognition product P′1 possesses 100-

Table 1 The OPA spectra of the probes and products in the presence of Pd^{2+} by TDDFT//M06-2X* (HF = 44%)/6-31+G(d)[a]

Mol.	λ^{o}_{max}/nm	f^{o}	Transition character	Mol.	λ^{o}_{max}/nm	f^{o}	Transition character
R1	445.0, 450 (ref. 14)	0.47	$S_0 \rightarrow S_1$ H $\rightarrow$ L 94.14%	P′1	385.6, 386 (ref. 12)	0.43	$S_0 \rightarrow S_1$ H $\rightarrow$ L 93.37%
R2	419.3	0.53	$S_0 \rightarrow S_1$ H $\rightarrow$ L 96.16%	P′2	367.3	0.50	$S_0 \rightarrow S_1$ H $\rightarrow$ L 95.74%
R3	460.9	0.45	$S_0 \rightarrow S_1$ H $\rightarrow$ L 95.27%	P′3	428.6	0.45	$S_0 \rightarrow S_1$ H $\rightarrow$ L 91.55%
R4	476.6	0.28	$S_0 \rightarrow S_1$ H $\rightarrow$ L 82.93%	P′4	451.0	0.24	$S_0 \rightarrow S_1$ H $\rightarrow$ L 89.35%
R5	379.8	1.05	$S_0 \rightarrow S_1$ H $\rightarrow$ L 96.85%	P′5	416.6, 450 (ref. 17)	0.97	$S_0 \rightarrow S_1$ H $\rightarrow$ L 97.04%
R6	376.0	1.22	$S_0 \rightarrow S_1$ H $\rightarrow$ L 97.19%	P′6	436.5	1.15	$S_0 \rightarrow S_1$ H $\rightarrow$ L 97.63%
R7	373.5	1.39	$S_0 \rightarrow S_1$ H $\rightarrow$ L 96.51%	P′7	452.2	1.25	$S_0 \rightarrow S_1$ H $\rightarrow$ L 96.54%
R8	433.7	1.00	$S_0 \rightarrow S_1$ H $\rightarrow$ L 98.60%	P′8	461.9	0.96	$S_0 \rightarrow S_1$ H $\rightarrow$ L 98.69%
R9	422.6	1.00	$S_0 \rightarrow S_1$ H $\rightarrow$ L 98.30%	P′9	471.7	1.00	$S_0 \rightarrow S_1$ H $\rightarrow$ L 98.43%

[a] H denotes the highest occupied molecular orbital, HOMO, and L is the lowest unoccupied molecular orbital, LUMO.

Table 2 The calculated K_r, K_{IC}, net-charge distribution, transferred charge, RMSD and vibrational relaxation energy of R1 and P′1[a]

	R1	P′1
	Weak fluorescence	Strong fluorescence (at 514 nm)
K_r	1.51×10^8 s^{-1}	1.52×10^8 s^{-1}
K_{IC}	2.00×10^{12} s^{-1}	3.05×10^7 s^{-1}
$Q(S_0)$	0.085 e	0.291 e
$Q(S_1)$	−0.178 e	0.191 e
q_{CT}	0.394 e	0.520 e
RMSD	0.228 Å	0.191 Å
ΔE_{vib}	0.43 eV	0.35 eV

[a] Q is the calculated net-charge distribution of the acetylene ether group (–OCH_2CCH) and hydroxyl group (–OH), respectively, shown in Fig. S5. q_{CT} is the transferred charge of the whole molecule from $S_0 \rightarrow S_1$. ΔE_{vib} is the vibrational relaxation energy in the excited state, that is, the energy difference between the vertical excited state and the adiabatic excited state of S_1.

fold fluorescence enhancement.[14] To explain the "turn-on" fluorescence change mechanism, we obtained the radiative decay rate K_r and internal conversion rate K_{IC} (the other non-radiative path could generally be ignored in the electronic transition) at a temperature of 298 K during the excited ground transition process by applying MOMAP software (detailed method description in the next section).[49–52] The calculated K_r values of R1 and P′1 are 1.51×10^8 s^{-1} and 1.52×10^8 s^{-1}, respectively, which are equal. However, the K_{IC} values are 2.00×10^{12} s^{-1} and 3.05×10^7 s^{-1} for probe R1 and product P′1, respectively, indicating that in probe R1, there would be weak fluorescence because the radiationless rate (2.00×10^{12} s^{-1}) is much larger than the radiative decay rate (1.51×10^8 s^{-1}). To further clarify the origin of the "turn-on" fluorescence, we also analysed the differences in electron properties, geometry variations, reorganization energies, Huang–Rhys factors (HR) and vibrational modes.

Firstly, the net-charge distributions on the acetylene ether group (–OCH_2CCH) and hydroxyl group (–OH), which are displayed in Table 2, are calculated based on nature bond orbital (NBO) analysis. It can be found that in the S_1 state, the –OCH_2CCH group exhibits electron-withdrawing character (−0.178 e); however, the –OH group shows electron-donating character (0.191 e). Meanwhile, the intramolecular charge transfer of the whole molecule associated with the ground and

Table 3 The fluorescence emission properties of probes R1–9 and products P′1–9 in the presence of Pd^{2+} by TDDFT//M06-2X* (HF = 44%)/6-31+G(d)

Mol.	λ^{e}_{max}/nm	f^{e}	Transition character	E^{0-0}/eV	τ/ns	K_r/s^{-1}	K_{IC}/s^{-1}
R1	510.2, —	0.59	$S_1 \rightarrow S_0$ L $\rightarrow$ H 98.34%	2.43	6.62	1.51×10^8	2.00×10^{12}
P′1	505.3, 514 (ref. 12)	0.58	$S_1 \rightarrow S_0$ L $\rightarrow$ H 98.34%	2.45	6.58	1.52×10^8	3.05×10^7
R2	455.7	0.32	$S_1 \rightarrow S_0$ L $\rightarrow$ H 98.24%	2.72	9.71	1.03×10^8	1.98×10^{11}
P′2	451.5	0.60	$S_1 \rightarrow S_0$ L $\rightarrow$ H 98.24%	2.75	5.10	1.96×10^8	1.05×10^{10}
R3	556.81	0.12	$S_1 \rightarrow S_0$ L $\rightarrow$ H 98.81%	2.23	38.5	0.26×10^8	4.38×10^{14}
P′3	575.9	0.38	$S_1 \rightarrow S_0$ L $\rightarrow$ H 98.79%	2.15	5.59	1.79×10^8	3.84×10^7
R4	574.7	0.04	$S_1 \rightarrow S_0$ L $\rightarrow$ H 98.18%	2.16	125	0.08×10^8	9.09×10^{11}
P′4	590.3	1.23	$S_1 \rightarrow S_0$ L $\rightarrow$ H 97.70%	2.10	4.24	2.36×10^8	1.28×10^6
R5	487.4	0.27	$S_1 \rightarrow S_0$ L $\rightarrow$ H 97.18%	2.54	13.2	0.76×10^8	9.89×10^{10}
P′5	483.6, 490 (ref. 17)	1.20	$S_1 \rightarrow S_0$ L $\rightarrow$ H 97.26%	2.56	2.92	3.42×10^8	2.64×10^7
R6	471.6	0.17	$S_1 \rightarrow S_0$ L $\rightarrow$ H 97.75%	2.63	19.6	0.51×10^8	5.96×10^9
P′6	508.0	1.37	$S_1 \rightarrow S_0$ L $\rightarrow$ H 97.81%	2.44	2.82	3.54×10^8	3.00×10^6
R7	462.6	0.07	$S_1 \rightarrow S_0$ L $\rightarrow$ H 97.80%	2.68	45.4	0.22×10^8	4.15×10^{10}
P′7	525.6	1.50	$S_1 \rightarrow S_0$ L $\rightarrow$ H 98.26%	2.36	2.76	3.62×10^8	7.51×10^6
R8	555.1	0.15	$S_1 \rightarrow S_0$ L $\rightarrow$ H 98.91%	2.23	31.2	0.32×10^8	1.46×10^9
P′8	552.7	1.09	$S_1 \rightarrow S_0$ L $\rightarrow$ H 98.96%	2.24	4.20	2.38×10^8	1.15×10^7
R9	532.4	0.26	$S_1 \rightarrow S_0$ L $\rightarrow$ H 98.85%	2.33	16.4	0.61×10^8	1.32×10^{10}
P′9	579.7	1.19	$S_1 \rightarrow S_0$ L $\rightarrow$ H 98.92%	2.14	4.24	2.36×10^8	3.75×10^6

excited states was obtained by a density-based approach, and is also displayed in Table 2. In the presence of Pd^{2+}, the $-OCH_2$-CCH group of probe R1 is hydrolyzed to the –OH of product P′1. The transferred charge was increased by the electron-donor –OH, such as P′1 (q_{CT} = 0.52 e) > R1 (q_{CT} = 0.39 e). The larger intramolecular charge transfer contributes to the easier electron transition and higher fluorescence efficiency. Additionally, the geometrical change of the stable ground state and lowest excited state for the two molecules was characterized by the root mean square displacement (RMSD) parameter, which can conveniently measure the overall degree of structural change. According to the geometry comparison simulation of the stable S_0 and S_1 states for R1 and P′1 shown in Fig. S6,† product P′1 is found to possess smaller geometrical change than probe R1, for example: P′1 (RMSD = 0.191) < R1 (RMSD = 0.228). Taking vertical excitation, the geometrical change mostly results from the geometrical relaxation of the excited state. The smaller geometrical relaxation of the excited state is beneficial for fluorescence enhancement by the reduction of radiationless energy. At the same time, the vibrational relaxation energies caused by the –OH group and the $-OCH_2CCH$ group were calculated. The results suggest that the –OH group of product P′1 caused smaller vibrational relaxation consumption than the $-OCH_2CCH$ group of probe R1 in the excited state, so largely reduced the vibrational relaxation energy, as displayed in Table 2 (ΔE(P′1): 0.35 eV < ΔE(R1): 0.43 eV), which alleviated the geometry distortion of product P′1 to achieve enhanced fluorescence efficiency. To the best of our knowledge, the Huang–Rhys factors (HR) can characterize the modifications of vibrational quanta (absorbed or emitted) when going from one electronic state to another, which are important for determining the K_{IC}.[53,54] It is calculated and clearly seen from Fig. 4 that (i) in general the HR factors for R1 (with a maximum value of 3.7) are much larger than those for P′1 (with a maximum value of 2.8) and (ii) the C≡C bond stretching modes of probe R1 appear at the 3255 cm^{-1} high frequency region, which further indicates that R1 has larger vibrational relaxation consumption. As a result, probe R1 shows weak fluorescence compared to product P′1, which successfully explains the experimental results.

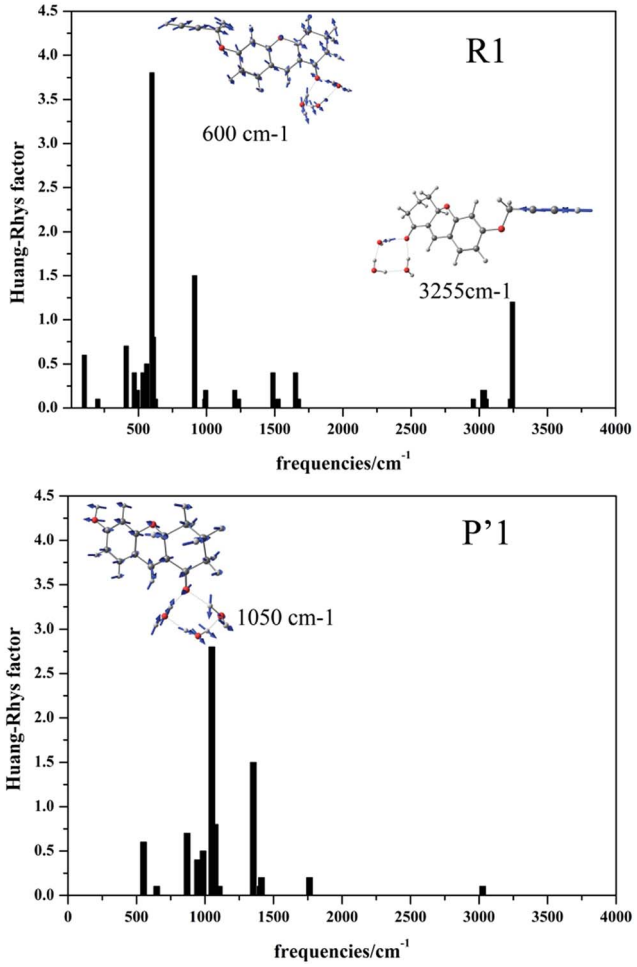

Fig. 4 Calculated Huang–Rhys factors *versus* the normal mode wave numbers and the normal mode displacement vectors for the strongest vibrations of R1 and P′1, respectively.

3.5. Fluorescence properties

Based on the stable excited-state geometry optimization using the TDDFT//M06-2X* (HF% = 44%)/6-31+G(d) method, the fluorescence properties of the studied molecules are calculated and are listed in Table 3, which also shows that the emission spectral scope is around 450–600 nm. The emission transitions of all the studied product compounds are assigned to $S_1 \rightarrow S_0$, composed of L → H. During the chemical modifications based on the coumarin core in this work, the changing trends of the emission spectra are in accordance with the results of the OPA spectra.

The fluorescence lifetime (τ) and fluorescence radiation rate (K_r) for spontaneous emission are calculated by employing the Einstein transition probabilities according to the formulae in (4) and (5),[55,56] and are also shown in Table 3:

$$\tau = \frac{c^3}{2(E_{Flu})^2 f^E} \quad (4)$$

$$K_r = \frac{1}{\tau} \quad (5)$$

Here, τ is the fluorescence lifetime, c stands for the velocity of light, E_{Flu} denotes the transition energy, f^E represents the oscillator strength of the emission spectra, and K_r is the rate of radiative decay.

In general, there are three major pathways for non-radiative decay for fluorescent molecules,[50] *i.e.* (i) internal conversion (IC) from S_1 to S_0, (ii) an intersystem crossing process (ISC) from a singlet manifold to a triplet, and (iii) charge separation (CS) during the photoisomerization process occurring in the excited state, often assisted by solvent. According to the analysis of the molecular structure (not heavy-atom) and electronic transition (mainly the $\pi \rightarrow \pi^*$ transition) of all the studied molecules, it would be difficult for the ISC process to happen. To further confirm the weak ISC process, we obtained the intersystem crossing rates (K_{ISC}) for $S_1 \rightarrow T_1$, shown in Table S7,† and the small K_{ISC} values implied that the ISC progress would be much

slower than the IC progress in this study. From Table S7,† we can also see that the $\Delta E_{S_1 \rightarrow T_1}$ values were large enough to inhibit the ISC process. Furthermore, the small effective spin–orbit coupling (SOC) matrix elements (below 1 cm^{-1}) reduced the K_{ISC} values significantly. The derivative details for K_{ISC} are shown in section B of the ESI.† Thus, here we focus on considering the influence of internal conversion non-radiative decay on the fluorescence efficiency of the studied molecules. Then, the final internal conversion rate (K_{IC}) from S_1 to S_0 is calculated with the Gaussian 09 program package using the formulae given by Shuai:[51]

$$K_{IC} = \frac{2\pi}{\hbar} R_{lk}{}^{f} Z_{iv}{}^{-1} \sum_{v_i, v_f} e^{-\beta E_{iv_i}} P_{lk}{}^{f} \delta\left(E_{if} + E_{iv_i} - E_{fv_f}\right) \quad (6)$$

$$R_{lk}{}^{f} = \langle \Phi_f | \hat{P}_{fl} | \Phi_i \rangle \langle \Phi_i | \hat{P}_{fk} | \Phi_f \rangle \quad (7)$$

$$P_{lk}{}^{f} = \langle \Theta_{fv_i} | \hat{P}_{fl} | \Theta_{iv_i} \rangle \langle \Theta_{iv_i} | \hat{P}_{fk} | \Theta_{fv_i} \rangle \quad (8)$$

where the non-radiative transition process is from an initial vibronic (excited) state $|iv\rangle$ to the final (ground) state $|fv\rangle$. $R_{lk}{}^{f}$ represents the coupling between the electronic wave functions of the two states. $|\Phi_i\rangle$ and $|\Phi_f\rangle$ denote the initial and final electronic states, respectively; $|\Theta_{iv_i}\rangle$ and $|\Theta_{fv_f}\rangle$ denote the vibrational states of the system and are expressed as the products of the wave functions of each normal mode. The calculated K_{IC} result (2.00×10^{12} s^{-1}) of probe R1 is much larger than its K_r value (1.51×10^{8} s^{-1}), which implied that the fluorescence of probe R1 is weak. After recognizing Pd^{2+}, the fluorescence radiation rate for the product P′1 ($K_r = 1.52 \times 10^{8}$ s^{-1}) is much larger than the non-radiation rate ($K_{IC} = 3.05 \times 10^{7}$ s^{-1}). Thus, the product P′1 shows brighter fluorescence, achieving "turn-on" fluorescence detection for Pd^{2+}. Similarly, it can be forecasted that the synthesized product P′5 would emit stronger fluorescence. The simulated results are in good agreement with the strong fluorescence phenomena seen from experiments. In addition, the excellent designed product P′4 (1.28×10^{6} s^{-1}) possesses a smaller K_{IC} than the corresponding probe R4 (9.09×10^{11} s^{-1}), which demonstrates that R4 could detect Pd^{2+} according to a "turn-on" fluorescence signal. Finally, for all the product molecules, except for P′2, the emission spectra are beyond 500 nm and possess strong fluorescent oscillator strengths and large K_r values ($\gg K_{IC}$), which demonstrate that these fluorescent molecules have the advantages of the smallest interference from autofluorescence and naked eye observation. These great fluorescent oscillator strengths and K_r values of the products should be ascribed to the stronger electron-donating (–OH) groups and better rigid conformations of the coumarin cores with smaller Huang–Rhys factors, which increase the intramolecular net-charge transfer and reduce the vibrational relaxation energy in the excited states, respectively, leading to strong fluorescence compared to the probe molecules.

3.6. Two-photon absorption (TPA) properties

As we know, practical application of a TP fluorescent probe in a biological system requires that the TP excited wavelength is located in the NIR spectral region (650–1200 nm). In order to evaluate the TP response for the studied product molecules, we perform calculations of the two-photon absorption (TPA) properties of the molecules, including the maximum cross-sections (δ^{T}_{max}) and corresponding TPA wavelengths (λ^{T}_{max}), by a TDDFT method in the 700–1200 nm region. Firstly, we obtain the TPA spectra of the synthesized P′1 by three functionals implemented in the DALTON program, which are described in Fig. S7.† It can be found from Fig. S7† that while different functionals are accompanied by little change the TPA intensity, there is some effect on the TPA wavelength. The peak position of P′1 calculated by the B3LYP (20% HF) functional is longer than that calculated by the BhandHLYP (50% HF) functional, which is mainly ascribed to the smaller Hartree–Fock percentage with the B3LYP functional. Compared with CAM-B3LYP, the result of B3LYP has a better agreement with the experimental results, which may be due to some error compensation that counteracts the long-range-corrected effect on the molecule. Thus, the B3LYP functional is expected to be more suitable for describing the TPA properties of these studied molecules according to comparisons with the experimental TP excited wavelengths and TPA cross-sections. Secondly, since a proper account of the solvent polarity effect is crucial for direct forecasts of the TPA properties, we also performed calculations on the λ^{T}_{max} and δ^{T}_{max} values of the synthesized P′1 molecules in solutions of different polarity (acetone ($\varepsilon = 4.2$), ethylcyanide ($\varepsilon = 36.34$), water ($\varepsilon = 78.39$)) and in the gas phase. To make the comparison more intuitive, the relationships between λ^{T}_{max} and δ^{T}_{max} are illustrated in Fig. 5. It can clearly be seen that the λ^{T}_{max} and δ^{T}_{max} values are affected upon adding polar solvents, which suggests that the solvent effect is not negligible. For this reason, in addition to using the PCM, the explicit water solvent effect was also considered in the TPA calculations for the studied molecules.

The calculations of the TPA properties of the studied compounds are implemented by applying the DALTON program at the same level, and the calculated results are listed in Table 4.

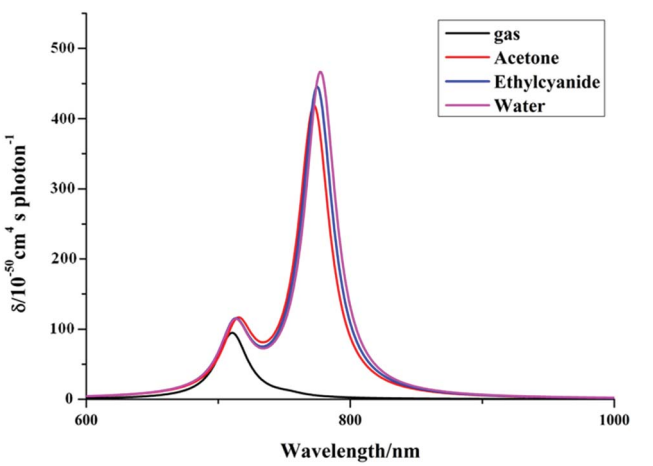

Fig. 5 Simulated TPA spectra of P′1 in solvents of different polarity by DALTON software (exp. λ^{T}_{max} = 820 nm, δ^{T}_{max} = 501 GM, order of solvent polarity: gas < acetone < ethylcyanide < water).

Table 4 The TPA properties of the studied products P′1–9 calculated by the DALTON program

Mol.	λ^{T}_{max}/nm	δ^{T}_{max}/GM	Transition character	σ
P′1	823.9, 820 (ref. 12)	534.31, 501 (ref. 12)	$S_0 \rightarrow S_1$	2.47, 2.32 (ref. 12)
P′2	770.2	246.87	$S_0 \rightarrow S_1$	1.06
P′3	835.0	845.87	$S_0 \rightarrow S_1$	2.95
P′4	1112.6	946.56	$S_0 \rightarrow S_1$	3.91
P′5	835.0, 800 (ref. 17)	215.20, 217 (ref. 17)	$S_0 \rightarrow S_1$	0.77, 0.78 (ref. 17)
P′6	839.0	437.49	$S_0 \rightarrow S_1$	1.67
P′7	840.7	613.32	$S_0 \rightarrow S_1$	1.96
P′8	988.0	700.58	$S_0 \rightarrow S_1$	2.44
P′9	1037.7	872.70	$S_0 \rightarrow S_1$	2.59

The calculated δ^{T}_{max} values of P′1 and P′5 by the TDDFT method are 534.31 GM at 823.9 nm and 215.20 GM at 835.0 nm, respectively, which are in good agreement with the experimental data (501 GM at 820 nm and 217 GM at 800 nm, respectively). As shown in Table 4, the λ^{T}_{max} values of the studied molecules range from 700 to 1200 nm, and the corresponding δ^{T}_{max} values are as large as 210–3800 GM. Remarkably, for the studied compounds, the maximum TPA responses are from the first excited states, and the corresponding transition is $S_0 \rightarrow S_1$.

According to the calculated results, P′4 bearing a cyano group as an acceptor at the 4-position has a much larger TPA cross-section than P′2 with a hydroxyl group as a donor at the 4-position, and P′3 containing a weaker electron-withdrawing chlorine at the 4-position, respectively. In addition to the effects of the electron-donating and electron-withdrawing influences, the π-conjugated structures also play important roles in the TPA properties of the studied compounds. From Table 4, it can be observed that P′6 with phenylacetylene as a π-conjugated structure displays 2-fold TPA cross-sections corresponding to those of P′5 with benzothiazolium. Furthermore, P′7 with a cyano group added on the phenylacetylene leads to a much longer TPA wavelength and larger cross-section than P′6. However, molecules with a large TPA cross-section per molecular weight ($\sigma = \delta_{max}$/MW) are essentially better for two-photon imaging detection.[57] Although molecules with a long π-conjugation chain also have a strong TP response, the big molecular weight of the long π-conjugation chain cannot contribute to δ_{max}/MW, such as in P′4 ($\sigma = 3.91$) > P′9 ($\sigma = 2.59$). What's more, molecules with δ_{max}/MW larger than 1.0 have been found to be useful for better applications.[58–60] In this regard, we are devoted to increasing the δ_{max}/MW values of the studied molecules to enable actual applications. As shown in Table 4, the two-photon cross-section per molecular weight σ values of all the designed molecules are over 1.5, except for that of P′2, indicating that the studied dyes have potential for Pd^{2+} recognition.

To further clarify the effects of internal factors on the TPA processes of these chromophores, in this subsection, we will focus on the main factors affecting the TPA process. Considering the strongest TPA transition, corresponding to $S_0 \rightarrow S_1$, the two-state (2S) approximation was adopted for an explanation of the calculated results. The model uses the two-state expression:[61]

$$\delta_{2S} = \frac{4|M_{0n}|^2|\Delta\mu_{0n}|^2}{15(E_{0n}/2)^2}\left(1 + 2\left(\cos\theta^{M_{0n}}_{\Delta\mu_{0n}}\right)^2\right) \quad (9)$$

where E is the corresponding excitation energy; M represents the transition dipole moment from the ground state to the TPA final state; $\Delta\mu$ denotes the state dipole moment difference between the ground state and the TPA final state; and the subscripts 0 and n stand for the ground state and the transition final state, respectively. $\theta^{M_{0n}}_{\Delta\mu_{0n}}$ is the angle between these two vectors. The approximate proportional relationship between δ^{T}_{max} and δ_{2S} during the TPA transition process (depicted in Fig. 6) implies that δ_{2S} can predict the changing tendency of δ^{T}_{max} in general.

According to the two-state expression, the δ^{T}_{max} values are largely determined by three parameters, which are calculated and the results are listed in Table 5. That is, (i) for all the studied compounds, the transition dipole moments M_{0n} and the state dipole moment differences $\Delta\mu_{0n}$ are critical factors influencing the δ^{T}_{max} values; the changing trends of the M_{01} and $\Delta\mu_{01}$ values are in accordance with those of the δ^{T}_{max} values. (ii) Compared with P′1 (534.31 GM), it can easily be observed that the M_{01} value of P′2 is much smaller than that of P′1, thus the decreased M_{01}

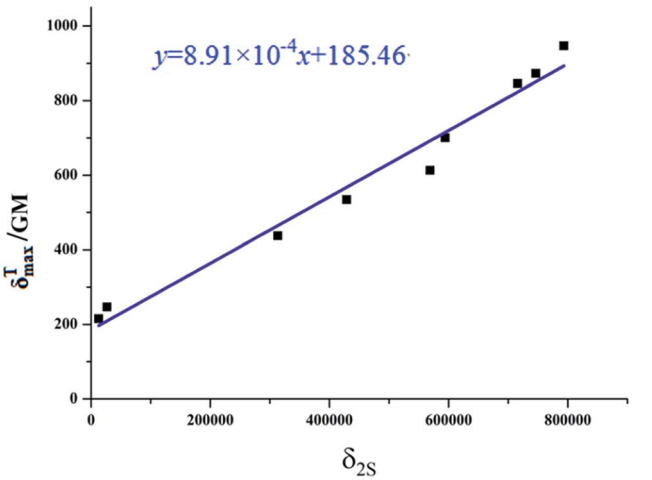

Fig. 6 Relationship plot of the maximum two-photon absorption cross-sections δ^{T}_{max} and δ_{2S} $\left[\frac{4|M_{0n}|^2|\Delta\mu_{0n}|^2}{15(E_{0n}/2)^2}(1 + 2(\cos\theta^{M_{0n}}_{\Delta\mu_{0n}})^2)\right]$ for all the studied product molecules.

Table 5 Important related parameters of the TPA properties of the studied product molecules P′1–9

Mol.	M_{01}	$\lvert\Delta\mu_{01}\rvert$	θ/°	E/eV	δ_{2S}	q_{CT}/e	d_{CT}/Å
P′1	6.70	5.89	25.52	2.95	428 934.2	0.521	0.851
P′2	4.09	4.55	88.08	3.21	26 604.86	0.503	1.694
P′3	7.92	7.38	35.06	2.97	715 805.3	0.609	1.859
P′4	8.60	7.62	38.23	3.09	793 553.7	0.708	2.461
P′5	2.13	4.14	62.32	2.62	12 808.38	0.447	0.036
P′6	11.4	5.17	48.64	2.97	313 567.6	0.435	0.834
P′7	10.5	7.20	77.28	2.95	568 973.5	0.528	1.750
P′8	7.90	7.05	63.67	2.39	594 192.7	0.521	0.805
P′9	10.6	7.85	88.02	2.71	746 409.8	0.769	1.201

value of P′2 should be responsible for its smaller δ^{T}_{max} value (246.87 GM). (iii) Adding an electron-withdrawing unit or increasing the electron-withdrawing ability at the 4-position leads to an obvious enhancement of both M_{0n} and δ^{T}_{max}, which results in an enhanced TPA response, for instance, P′1 (6.70 Debye, 534.31 GM) < P′3 (7.92 Debye, 845.87 GM), P′1 (6.70 Debye, 534.31 GM) < P′4 (8.60 Debye, 946.56 GM). Notably, this similar changing trend also occurs in P′6 and P′8, so we can rationally elucidate that adding an acceptor unit or increasing the electron-withdrawing ability at the 4-position is favorable for the TPA response enhancement of coumarin derivative dyes. (iv) Comparing P′5 and P′6, it can be found that replacing the benzothiazolium moiety by a phenylacetylene group can obviously increase the δ^{T}_{max} values of the compounds, which is attributed to the largely increased $\Delta\mu_{01}$ and M_{01} values of the compounds with phenylacetylene units.

Overall, the above results show that the state dipole moment difference $\Delta\mu_{0n}$ plays a dominant role in the TPA properties. To the best of our knowledge, the state dipole moment difference $\Delta\mu_{0n}$ is closely related to the charge-transfer distance (d_{CT}) and the transferred charge (q_{CT}), as presented in the expression:[41]

$$\Delta\mu \propto d_{CT} \times q_{CT} \quad (10)$$

Here, $\Delta\mu$ is the difference of the dipole moments computed for the ground and the excited states; d_{CT} stands for the spatial distance between the two barycenters of the density distributions, *i.e.* the charge-transfer distance. q_{CT} represents the transferred charge during the transition process. It has been shown that this density-based approach is much more meaningful than a charge-based approximation.[42] The calculated results of d_{CT} and q_{CT} are also shown in Table 5. It is found that introducing an acceptor at the 4-position leads to larger q_{CT} and d_{CT} values, such as P′3 (0.609 e, 1.859 Å) > P′1 (0.521 e, 0.851 Å). Furthermore, the q_{CT} and d_{CT} values are larger for stronger acceptors, such as P′4 (0.708 e, 2.461 Å) > P′3 (0.609 e, 1.859 Å). Importantly, upon extending the conjugation length, the d_{CT} value is markedly increased, such as P′6 (0.834 Å) > P′5 (0.036 Å), which results in a TPA transition enhancement, P′6 (437.49 GM) > P′5 (215.20 GM). In conclusion, introducing an electron-withdrawing group or increasing the electron-withdrawing ability at the 4-position of the coumarin core can effectively enlarge the charge-transfer distance (d_{CT}) and transferred charge (q_{CT}); extending the conjugation length at the 3-position of the coumarin core can significantly increase the charge-transfer distance (d_{CT}), and all this leads to larger δ^{T}_{max} values in the NIR region.

4. Conclusions

In the present study, we provided some strategies for designing a series of two-photon (TP) fluorescent palladium ion (Pd^{2+}) probes and the corresponding product molecules by chemical modification, and firstly systematically and deeply investigated their electronic structures and one-photon absorption (OPA), fluorescence emission and two-photon absorption (TPA) optical properties from a theoretical viewpoint. Moreover, the radiative and non-radiative behaviors for the synthesized probe R1 (K_r: 1.51×10^8 s^{-1} $\ll$ K_{IC}: 2.00×10^{12} s^{-1}) and the synthesized product P′1 (K_r: 1.52×10^8 s^{-1} $\cong$ K_{IC}: 3.05×10^7 s^{-1}) have been revealed quantitatively and qualitatively. These are due to the presence of an auxochromic and electron-donating –OH group in the product molecule replacing a large $-OCH_2CCH$ group in the probe, reducing the geometrical relaxation and vibrational relaxation energies in the excited states and increasing intramolecular charge transfer. On the basis of the synthesized P′1 (GCTPOC) and P′5 (TPF) cores, it is easier to effectively increase the TP absorption cross-section per molecular weight by introducing an electron-withdrawing group (–Cl or –CN) to the 4-position than by extending the π-conjugated structure at the 3-position. Further investigations show that both introducing an electron-withdrawing group or increasing the electron-withdrawing ability at the 4-position, and extending the π-conjugated structure at the 3-position of the coumarin core with phenylethylene, result in small H → L energy gaps, a red-shift of the absorption and emission spectra, the enhancement of δ^{T}_{max}, and larger transition dipole moments. By introducing chlorine and cyano substituents at the 4-position in the central coumarin skeleton, the molecules P′3 and P′4 display obvious bathochromic shifts of λ^{T}_{max} and increased δ^{T}_{max} and transition dipole moments relative to those of P′1, which are ascribed to the strong electron-withdrawing ability increasing the charge transfer q_{CT}. On the other hand, incorporating the π-extended structure of phenylethylene at the 3-position of the coumarin core (P′6) leads to a red-shift of the OPA and fluorescence emission bands, and a 222 GM enhancement of δ^{T}_{max} relative to P′5, which is attributed to the extended π-conjugated structure enlarging the charge-transfer distance d_{CT}. For the fluorescence performances, except for product P′2, the emission spectra of the other products are beyond 500 nm and possess strong fluorescent oscillator strengths and large K_r values ($\gg K_{IC}$), which demonstrate that the designed Pd^{2+} TP probes could realize Pd^{2+} detection according to the "turn-on" fluorescence. Consequently, P′4, with a much smaller K_{IC} (1.28×10^6 s^{-1}) than R4 (9.09×10^{11} s^{-1}), possesses the largest TPA cross-section per molecular weight (3.91) and the longest fluorescence wavelength (590.3 nm) among all the studied molecules. Considering these outstanding properties of product P′4, the Pd^{2+} probe R4 may be the most promising candidate for Pd^{2+} detection. Finally, we hope that this theoretical investigation of

the coumarin-based TP strategy might also provide useful information for further studies on Pd^{2+} detection.

Conflicts of interest

There are no conflicts to declare.

Acknowledgements

This work was supported by the Natural Science Foundation of China (No. 21473071, 21173099, 20973078 and 11404041), the Major State Basis Research Development Program (Grant 2013CB 834801), and special funding for basic scientific research projects for Central Colleges.

References

1 B. Liu, H. Wang, T. Wang, Y. Bao, F. Du, J. Tian, Q. Li and R. Bai, A new ratiometric ESIPT sensor for detection of palladium species in aqueous solution, *Chem. Commun.*, 2012, **48**, 2867–2869.

2 B. Liu, Y. Bao, F. Du, H. Wang, J. Tian and R. Bai, Synthesis and characterization of a fluorescent polymer containing 2,6-bis(2-thienyl)pyridine moieties as a highly efficient sensor for Pd^{2+} detection, *Chem. Commun.*, 2011, **47**, 1731–1733.

3 C. D. Spicer, T. Triemer and B. G. Davis, Palladium-mediated cell-surface labeling, *J. Am. Chem. Soc.*, 2012, **134**, 800–803.

4 R. M. Yusop, A. Unciti-Broceta, E. M. V. Johansson, R. M. Sanchez-Martin and M. Bradley, Palladium-mediated intracellular chemistry, *Nat. Chem.*, 2011, **3**, 239–243.

5 C. E. Garrett and K. Prasad, The Art of Meeting Palladium Specifications in Active Pharmaceutical Ingredients Produced by Pd-Catalyzed Reactions, *Adv. Synth. Catal.*, 2004, **346**, 889–900.

6 L. Zhou, Q. Wang, X. B. Zhang and W. Tan, Through-bond energy transfer-based ratiometric two-photon probe for fluorescent imaging of Pd^{2+} ions in living cells and tissues, *Anal. Chem.*, 2015, **87**, 4503–4507.

7 H. Chen, W. Lin and L. Yuan, Construction of a near-infrared fluorescence turn-on and ratiometric probe for imaging palladium in living cells, *Org. Biomol. Chem.*, 2013, **11**, 1938–1941.

8 W. Liu, J. Jiang, C. Chen, X. Tang, J. Shi, P. Zhang, K. Zhang, Z. Li, W. Dou, L. Yang and W. Liu, Water-soluble colorimetric and ratiometric fluorescent probe for selective imaging of palladium species in living cells, *Inorg. Chem.*, 2014, **53**, 12590–12594.

9 B. Zhu, C. Gao, Y. Zhao, C. Liu, Y. Li, Q. Wei, Z. Ma, B. Du and X. Zhang, A 4-hydroxynaphthalimide-derived ratiometric fluorescent chemodosimeter for imaging palladium in living cells, *Chem. Commun.*, 2011, **30**, 8656–8658.

10 R. O'Kennedy and R. D. Thornes, *Coumarins: Biology, Applications and Mode of Actions*, John Wiley and Sons, Chichester, 1997.

11 M. Tasior, D. Kim, S. Singha, M. Krzeszewski, K. H. Ahn and D. T. Gryko, π-Expanded coumarins: synthesis, optical properties and applications, *J. Mater. Chem. C*, 2015, **3**, 1421–1446.

12 L. Yuan, W. Lin, H. Chen, S. Zhu and L. He, A unique family of rigid analogues of the GFP chromophore with tunable two-photon action cross-sections for biological imaging, *Angew. Chem., Int. Ed.*, 2013, **52**, 10018–10022.

13 Y. H. Lee, W. X. Ren, J. Han, K. Sunwoo, J. Y. Lim, J. H. Kim and J. S. Kim, Highly selective two-photon imaging of cysteine in cancerous cells and tissues, *Chem. Commun.*, 2015, **51**, 14401–14404.

14 H. Cui, H. Chen, Y. Pan and W. Lin, A two-photon fluorescent turn-on probe for palladium imaging in living tissues, *Sens. Actuators, B*, 2015, **219**, 232–237.

15 K. Zheng, W. Lin, D. Cheng, H. Chen, Y. Liu and K. Liu, A two-photon fluorescent turn-on probe for nitroxyl (HNO) and its bioimaging application in living tissues, *Chem. Commun.*, 2015, **51**, 5754–5757.

16 K. Zheng, W. Lin, L. Tan and D. Cheng, A two-photon fluorescent probe with a large turn-on signal for imaging hydrogen sulfide in living tissues, *Anal. Chim. Acta*, 2015, **853**, 548–554.

17 Q. Chen, J. Yang, Y. Li, J. Zheng and R. Yang, Sensitive and rapid detection of endogenous hydrogen sulfide distributing in different mouse viscera via a two-photon fluorescent probe, *Anal. Chim. Acta*, 2015, **896**, 128–136.

18 L. Duan, Y. Xu and X. Qian, Highly sensitive and selective Pd^{2+} sensor of naphthalimide derivative based on complexation with alkynes and thio-heterocycle, *Chem. Commun.*, 2008, **47**, 6339–6341.

19 M. Kumar, N. Kumar and V. Bhalla, Highly selective fluorescent probe for detection and visualization of palladium ions in mixed aqueous media, *RSC Adv.*, 2013, **3**, 1097–1102.

20 M. Santra, S. K. Ko, I. Shin and K. H. Ahn, Fluorescent detection of palladium species with an O-propargylated fluorescein, *Chem. Commun.*, 2010, **46**, 3964–3966.

21 M. Pal, K. Parasuraman and K. R. Yeleswarapu, Palladium-catalyzed cleavage of O/N-propargyl protecting groups in aqueous media under a copper-free condition, *Org. Lett.*, 2003, **5**, 349–352.

22 S. Huang, L. Y. Zou, A. M. Ren, J. F. Guo, X. T. Liu, J. K. Feng and B. Z. Yang, Computational design of two-photon fluorescent probes for a zinc ion based on a salen ligand, *Inorg. Chem.*, 2013, **52**, 5702–5713.

23 X. Liu, J. Zhang, K. Li, X. Sun, Z. Wu, A. Ren and J. Feng, New insights into two-photon absorption properties of functionalized aza-BODIPY dyes at telecommunication wavelengths: a theoretical study, *Phys. Chem. Chem. Phys.*, 2013, **15**, 4666–4676.

24 D. Wang, J. F. Guo, A. M. Ren, S. Huang, L. Zhang and J. K. Feng, Computational design of two-photon fluorescent probes for intracellular free zinc ions, *J. Phys. Chem. B*, 2014, **118**, 10101–10110.

25 Z. Xu, A. M. Ren, D. Wang, J. F. Guo, J. K. Feng and X. Yu, A theoretical investigation on two latest two-photon pH fluorescent probes, *J. Photochem. Photobiol., A*, 2014, **293**, 50–56.

26 R. Feng, Y. Sun, M. Tian, G. Zhang, R. Zhang, L. Guo, X. Li, X. Yu and N. Zhao, A membrane-permeable dye for living cells with large two-photon excited fluorescence action cross-sections for bioimaging, *J. Mater. Chem. B*, 2015, **44**, 8644–8649.

27 F. Miao, W. Zhang, Y. Sun, R. Zhang, Y. Liu, F. Guo, G. Song, M. Tian and X. Yu, Novel fluorescent probes for highly selective two-photon imaging of mitochondria in living cells, *Biosens. Bioelectron.*, 2014, **55**, 423–429.

28 C. Zhang, L. Y. Zou, D. Wang, L. Zhang and A. M. Ren, A theoretical investigation and design of fluorescent probes with large two-photon absorption cross-sections and dual signaling behavior for mercury ions in biological system, *J. Photochem. Photobiol., A*, 2017, **332**, 440–452.

29 V. M. Aleksandr, J. C. Christopher and G. T. Donald, Universal Solvation Model Based on Solute Electron Density and on a Continuum Model of the Solvent Defined by the Bulk Dielectric Constant and Atomic Surface Tensions, *J. Phys. Chem. B*, 2009, **113**, 6378–6396.

30 A. D. Becke, Density-functional thermochemistry. III. The role of exact exchange, *J. Chem. Phys.*, 1993, **98**, 5648–5652.

31 A. D. Becke, Density-functional thermochemistry. IV. A new dynamical correlation functional and implications for exact-exchange mixing, *J. Chem. Phys.*, 1996, **104**, 1040–1046.

32 Y. Zhao and D. G. Truhlar, The M06 suite of density functionals for main group thermochemistry, thermochemical kinetics, noncovalent interactions, excited states, and transition elements: two new functionals and systematic testing of four M06-class functionals and 12 other functionals, *Theor. Chem. Acc.*, 2008, **120**, 215–241.

33 D. Wang, A. M. Ren, J. F. Guo, L. Y. Zou and S. Huang, Computational design of a two-photon excited FRET-based ratiometric fluorescent Cu^{2+} probe for living cell imaging, *RSC Adv.*, 2015, **5**, 98144–98153.

34 N. S. Makarov, S. Mukhopadhyay, K. Yesudas, J. L. Brédas, J. W. Perry, A. Pron, M. Kivala, K. Mullen, A. Pron, M. Kivala and K. Müllen, Impact of electronic coupling, symmetry, and planarization on one and two-photon properties of triarylamines with one, two, or three diarylboryl acceptors, *J. Phys. Chem. A*, 2012, **116**, 3781–3793.

35 X. Wang, F. Q. Bai, Y. Liu, Y. Wang, H. X. Zhang and Z. Lin, A computational way to achieve more effective candidates for photodynamic therapy, *J. Chem. Inf. Model.*, 2017, **57**, 1089–1100.

36 M. J. Frisch, G. W. Trucks, H. B. Schlegel, G. E. Scuseria, M. A. Robb, J. R. Cheeseman, G. Scalmani, V. Barone, B. Mennucci and G. A. Petersson, *et al.*, *Gaussian 09, revisions A.02 and B.01*, Gaussian, Inc., Wallingford, CT, 2009.

37 DALTON, a molecular electronic structure program, Release Dalton2011, see http://daltonprogram.org/.

38 Y. Luo, P. Norman, P. Macak and H. Ågren, Solvent-induced two-photon absorption of a push−pull molecule, *J. Phys. Chem. A*, 2000, **104**, 4718–4722.

39 W. M. Mcclain, Excited state symmetry assignment through polarized two-photon absorption studies of fluids, *J. Chem. Phys.*, 1971, **55**, 2789–2796.

40 M. Albota, D. Beljonne, J. L. Bredas, J. E. Ehrlich, J. Y. Fu, A. A. Heikal, S. E. Hess, T. Kogej, M. D. Levin, S. R. Marder, *et al.*, Design of organic molecules with large two-photon absorption cross sections, *Science*, 1998, **281**, 1653–1656.

41 T. L. Bahers, C. Adamo and I. Ciofini, A qualitative index of spatial extent in charge-transfer excitations, *J. Chem. Theory Comput.*, 2011, **7**, 2498–2506.

42 B. L. Guennic, S. Chibani, A. Charaf-Eddin, J. Massue, R. Ziessel, G. Ulrich and D. Jacquemin, The NBO pattern in luminescent chromophores: unravelling excited-state features using TD-DFT, *Phys. Chem. Chem. Phys.*, 2013, **15**, 7534–7540.

43 L. Yuan, L. Wang, B. K. Agrawalla, S. J. Park, H. Zhu, B. Sivaraman, J. Peng, Q. H. Xu and Y. T. Chang, Development of targetable two-photon fluorescent probes to image hypochlorous acid in mitochondria and lysosome in live cell and inflamed mouse model, *J. Am. Chem. Soc.*, 2015, **137**, 5930–5938.

44 H. Ammar, S. Abid and S. Fery-Forgues, Synthesis and spectroscopic study of new biscoumarin dyes based on 7-(4-methylcoumarinyl) diesters, *Dyes Pigm.*, 2008, **78**, 1–7.

45 K. Żamojć, W. Wiczk, B. Zaborowski, D. Jacewicz and L. Chmurzyński, Fluorescence quenching of 7-amino-4-methylcoumarin by different TEMPO derivatives, *Spectrochim. Acta, Part A*, 2015, **136**, 1875–1880.

46 A. Matta, V. Bahadur, T. Taniike, J. Van der Eycken and B. K. Singh, Synthesis, characterisation and photophysical studies of oxadiazolyl coumarin: a new class of blue light emitting fluorescent dyes, *Dyes Pigm.*, 2017, **140**, 250–260.

47 B. Zhu, W. Wang, L. Liu, H. Jiang, B. Du and Q. Wei, A highly selective colorimetric and long-wavelength fluorescent probe for Hg^{2+}, *Sens. Actuators, B*, 2014, **191**, 605–611.

48 Ł. G. Łukasiewicz, I. Deperasińska, Y. M. Poronik, Y. W. Jun, M. Banasiewicz, B. Kozankiewicz, K. H. Ahn and D. T. Gryko, Dipolar Dyes with a Pyrrolo[2,3-b]quinoxaline Skeleton Containing a Cyano Group and a Bridged Tertiary Amino Group: Synthesis, Solvatofluorochromism, and Bioimaging, *Chem.–Asian J.*, 2016, **11**, 1718–1724.

49 Q. Peng, Y. Yi, Z. Shuai and J. Shao, Excited state radiationless decay process with Duschinsky rotation effect: formalism and implementation, *J. Chem. Phys.*, 2007, **126**, 114302.

50 Q. Peng, Y. Yi, Z. Shuai and J. Shaooward, Quantitative Prediction of Molecular Fluorescence Quantum Efficiency: Role of Duschinsky Rotation, *J. Am. Chem. Soc.*, 2007, **129**, 9333–9339.

51 Y. Niu, Q. Peng and Z. Shuai, Promoting-mode free formalism for excited state radiationless decay process with Duschinsky rotation effect, *Sci. China, Ser. B: Chem.*, 2008, **51**, 1153–1158.

52 Y. Niu, Q. Peng, C. Deng, X. Gao and Z. Shuai, Theory of excited state decays and optical spectra: application to polyatomic molecules, *J. Phys. Chem. A*, 2010, **114**, 7817–7831.

53 S. Yin, Q. Peng, Z. Shuai, W. Fang, Y. H. Wang and Y. Luo, Aggregation-enhanced luminescence and vibronic coupling

of silole molecules from first principles, *Phys. Rev. B: Condens. Matter Mater. Phys.*, 2006, **73**, 205409.

54 G. Yu, S. Yin, Y. Liu, J. Chen, X. Xu, X. Sun, D. Ma, X. Zhan, Q. Peng, Z. Shuai, B. Tang, D. Zhu, W. Fang and Y. Luo, Structures, Electronic States, Photoluminescence, and Carrier Transport Properties of 1,1-Disubstituted 2,3,4,5-Tetraphenylsiloles, *J. Am. Chem. Soc.*, 2005, **127**, 6335–6346.

55 V. Lukeš, A. Aquino and H. Lischka, Theoretical Study of Vibrational and Optical Spectra of Methylene-Bridged Oligofluorenes, *J. Phys. Chem. A*, 2005, **109**, 10232–10238.

56 X. Liu, J. Guo, A. Ren, Z. Xu, S. Huang and J. Feng, Theoretical insight into linear optical and two-photon absorption properties for a series of N-arylpyrrole-based dyes, *Org. Biomol. Chem.*, 2012, **10**, 7527–7535.

57 H. M. Kim and B. R. Cho, Two-photon materials with large two-photon cross sections: structure-property relationship, *Chem. Commun.*, 2009, **2**, 153–164.

58 H. M. Kim, C. Jung, B. R. Kim, S. Y. Jung, J. H. Hong, Y. G. Ko, K. J. Lee and B. R. Cho, Environment-sensitive two-photon probe for intracellular free magnesium ions in live tissue, *Angew. Chem., Int. Ed.*, 2007, **46**, 3460–3463.

59 H. M. Kim, B. R. Kim, J. H. Hong, J. S. Park, K. J. Lee and B. R. Cho, A two-photon fluorescent probe for calcium waves in living tissue, *Angew. Chem., Int. Ed.*, 2007, **46**, 7445–7448.

60 B. H. Cumpston, S. P. Ananthavel, S. Barlow, D. L. Dyer, J. E. Ehrlich, L. L. Erskine, A. A. Heikal, S. M. Kuebler, I. Y. S. Lee, D. McCord-Maughon, J. Qin, H. Rockel, M. Rumi, X. L. Wu, S. R. Marderk and J. W. Perry, Two-photon polymerization initiators for three dimensional optical data storage and microfabrication, *Nature*, 1999, **398**, 51–54.

61 N. A. Murugan, R. Zaleśny, J. Kongsted, A. Nordberg and H. Ågren, Promising two-photon probes for in vivo detection of β amyloid deposits, *Chem. Commun.*, 2014, **50**, 11694–11697.